RSC Advances

PAPER

View Article Online
View Journal | View Issue

Cite this: *RSC Adv.*, 2019, **9**, 41058

Electronic and optical properties of Janus ZrSSe by density functional theory

Tuan V. Vu,[ab] Hien D. Tong,[c] Duy Phu Tran,[d] Nguyen T. T. Binh,*[e] Chuong V. Nguyen,[f] Huynh V. Phuc,[g] Hoat M. Do[h] and Nguyen N. Hieu*[e]

In the present work, we investigate systematically the electronic and optical properties of Janus ZrSSe using first-principles calculations. Our calculations demonstrate that the Janus ZrSSe monolayer is an indirect semiconductor at equilibrium. The band gap of the Janus ZrSSe is 1.341 eV using the Heyd–Scuseria–Ernzerhof hybrid functional, larger than the band gap of $ZrSe_2$ monolayer and smaller than that of ZrS_2 monolayer. Based on the analysis of the band edge alignment, we confirm that the Janus ZrSSe monolayer possesses photocatalytic activities that can be used in water splitting applications. While strain engineering plays an important role in modulating the electronic properties and optical characteristics of the Janus ZrSSe monolayer, the influence of the external electric field on these properties is negligible. The biaxial strain, ε_b, has significantly changed the band of the Janus ZrSSe monolayer, and particularly, the semiconductor–metal phase transition which occurred at $\varepsilon_b = 7\%$. The Janus ZrSSe monolayer can absorb light in both visible and ultraviolet regions. Also, the biaxial strain has shifted the first optical gap of the Janus ZrSSe monolayer. Our findings provide additional information for the prospect of applying the Janus ZrSSe monolayer in nanoelectronic devices, especially in water splitting technology.

Received 21st October 2019
Accepted 28th November 2019

DOI: 10.1039/c9ra08605f

rsc.li/rsc-advances

1 Introduction

Since the successful separation in 2004, graphene has become one of the top materials of interest to the scientific community due to its many extraordinary chemical and physical properties.[1] The success of graphene in nanotechnology applications has led to a wide search for two-dimensional (2D) layered materials. In fact, many 2D graphene-like materials have been systematically studied, such as silicene, germanene, phosphorene and transition metal dichalcogenides,[2–6] and in particular, van der Waals heterostructures.[7–10] Recently, the Janus MoSSe monolayer, a new type of asymmetric transition metal dichalcogenide, was successfully synthesized through chemical vapour deposition.[11,12] This has opened a new direction in the study of 2D materials. Several theoretical studies have focused on monolayers of Janus transition metal dichalcogenides[13] and Janus monochalcogenide.[14] The breaking of mirror symmetry in Janus transition metal dichalcogenides, which has been confirmed by scanning transmission electron microscopy,[12] has given rise to many new physical properties with many promising applications in nanoelectronic and energy storage technologies.[13,15,16]

Monolayer ZrS_2 has been experimentally synthesized by Zeng and co-workers.[17] Both ZrS_2 and $ZrSe_2$ are indirect semiconductors from first-principles calculations.[15,18] Similar to other 2D layered materials, the electronic properties of the ZrS_2 and $ZrSe_2$ monolayers are very sensitive to external influences.[19] Xin and co-workers indicated that semiconductor–metal transition was found at large elongation of biaxial strain.[20] Besides, strain engineering can also lead to indirect–direct band gap in the ZrS_2 monolayer.[21] By replacing the bottom layer of S(Se) atoms in monolayer ZrS_2($ZrSe_2$) with Se(S) atoms, we obtain the structure of the Janus ZrSSe monolayer. Using first-principles calculations, Guo and co-workers show that the Janus ZrSSe, an indirect semiconductor, is mechanically and dynamically stable.[18] Janus ZrSSe may possess photocatalytic activities due to its high asymmetric arrangement.[15] Also, the breaking of the inversion symmetry in the Janus structure of ZrSSe leads to a significant change in its piezoelectricity.[22] It is well-known that spin–orbit coupling (SOC) plays an important role in the

[a]*Division of Computational Physics, Institute for Computational Science, Ton Duc Thang University, Ho Chi Minh City, Viet Nam. E-mail: vuvantuan@tdtu.edu.vn*

[b]*Faculty of Electrical & Electronics Engineering, Ton Duc Thang University, Ho Chi Minh City, Viet Nam*

[c]*Faculty of Engineering, Vietnamese-German University, Binh Duong, Viet Nam*

[d]*Future Industries Institute, ARC Centre of Excellence in Convergent Bio-Nano Science and Technology, University of South Australia, Mawson Lakes, Campus Mawson Lakes, South Australia 5095, Australia*

[e]*Institute of Research and Development, Duy Tan University, Da Nang 550000, Viet Nam. E-mail: nguyentthanhbinh8@duytan.edu.vn; hieunn@duytan.edu.vn*

[f]*Department of Materials Science and Engineering, Le Quy Don Technical University, Ha Noi 100000, Viet Nam*

[g]*Division of Theoretical Physics, Dong Thap University, Dong Thap, Viet Nam*

[h]*Computational Laboratory for Advanced Materials and Structures, Advanced Institute of Materials Science, Ton Duc Thang University, Ho Chi Minh City, Viet Nam*

electronic properties of layered materials.[23,24] When the SOC is included, the band gap of the Janus SnSSe[24] and Janus transition metal dichalchogenide[23] monolayers is reduced and a spin–orbit splitting was found at the Γ-point. This indicates that the spin–orbit splitting value depends strongly on the strain engineering.

In the present work, we focus on the electronic and optical properties of the Janus ZrSSe using first-principles calculations. To get a high level of accuracy in the energy gap problem, we used different functionals in our calculations. We also compared the results obtained from Janus ZrSSe with ZrS_2 and $ZrSe_2$ monolayers. The photocatalytic characteristics and catalytic activities of the Janus ZrSSe were also checked. The effects of strain engineering and the external electric field on the electronic and optical properties of the Janus ZrSSe have also been systematically studied in this work.

2 Computational details

In this study, all calculations are performed using density functional theory (DFT), which is implemented in the Quantum Espresso package[25] within the projected augmented wave (PAW) method.[26] The generalized gradient approximation (GGA) suggested by Perdew, Burke, and Ernzerhof (PBE)[27,28] is chosen to describe the exchange–correction functional, and the SOC is included self consistently.[29] Also, the Heyd–Scuseria–Ernzerhof (HSE06) hybrid functional[30] is used to solve the problems of band structure and band gap of the monolayers ZrS_2, $ZrSe_2$, and Janus ZrSSe. A semi-empirical DFT-D2 method proposed by Grimme[31] is used to consider the long-range weak van der Waals interactions which exist in the monolayers. The cut-off energy is set to 500 eV, and the Brillouin zone is sampled by a $12 \times 12 \times 1$ k-point grid. All the atoms are fully relaxed until the residue forces on each atom and total energy are converged to 0.001 eV $Å^{-1}$ and 10^6 eV, respectively. To eliminate the interactions between neighbour layers, a vacuum space of 20 Å along the c-axis (perpendicular to the monolayer surface) is used.

For calculations of the optical properties, we focus only on the dielectric function $\varepsilon(\omega)$ and the absorption coefficient $\alpha(\omega)$ of the Janus ZrSSe monolayer. The imaginary part of the $\varepsilon(\omega)$ can be estimated *via* the sum of the transitions between occupied and unoccupied states and the real part can be calculated through the Kramers–Kronig relation.

To consider the effect of a biaxial strain on electronic and optical properties of monolayers ZrS_2, $ZrSe_2$, and Janus ZrSSe, we defined the strain elongation ε_b as $\varepsilon_b = (l - l_0)/l_0$, where l_0 and l are, respectively, the lattice constants of pristine and strained monolayers. The plus and minus signs refer, respectively, to the tensile and compressive biaxial strains. To consider the influence of an electric field on the electronic and optical properties of the monolayers ZrS_2, $ZrSe_2$, and Janus ZrSSe, an electric field E is applied perpendicular to the 2D plane of the monolayers (c-axis). The negative field is applied so that the direction of the E is opposite to the positive direction of the c-axis. In this work, the applied biaxial strain, ε_b, is from −8% to 8% and the value of the external electric field is up to 5 V nm^{-1}.

3 Results and discussion

The optimized atomic structure of Janus ZrSSe is shown in Fig. 1(a). We can build the structure of the Janus ZrSSe from the well-known $ZrSe_2$ structure[32] by replacing the bottom or top layer of the Se atoms by S atoms. The atomic structure of the $ZrSe_2$ or ZrS_2 monolayers belongs to the group symmetry $P3m1$. Replacing the Se by S atoms results in distortion of the out-of-plane symmetry of the Janus ZrSSe. This causes the mirror symmetry to be broken with the absence of mirror planes perpendicular to the c-axis. The Janus ZrSSe belongs to a non-centrosymmetric group with space group symmetry $P3m1$. The structural parameters of the Janus ZrSSe, $ZrSe_2$ and ZrS_2 monolayers are listed in Table 1. After optimization, the lattice constant of Janus ZrSSe is $a = 3.738$ Å. This value is larger than the lattice constant of monolayer ZrS_2 but smaller than that of monolayer $ZrSe_2$. The bond lengths between the Zr atom and the S and Se atoms in the Janus ZrSSe are $d_{Zr-S} = 2.572$ Å and $d_{Zr-Se} = 2.705$ Å. Our obtained results are in good agreement with previous DFT calculations.[18,22] Also, we have calculated the charge density as shown in Fig. 1(b) and (c). Previously, electrostatic potential differences at the surface of 2D Janus structures have been observed.[33] We know that the difference in electrostatic potential can lead to a difference in the redox potential. This is very important in finding applicability in water splitting technology. In Fig. 2(a), we show the electrostatic

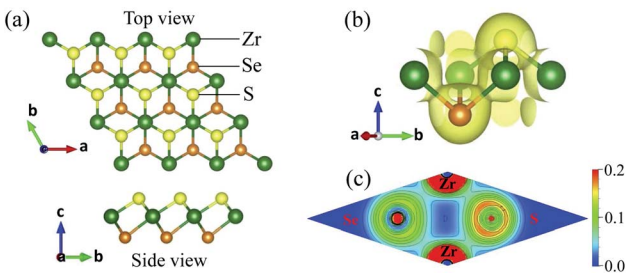

Fig. 1 (a) Optimized atomic structure of Janus ZrSSe, (b) charge density in the Janus ZrSSe with isolated 0.04, and (c) electron density of atoms in contour form from 0 to 0.2 e $Bohr^{-3}$ with the interval of 0.02 $Bohr^3$.

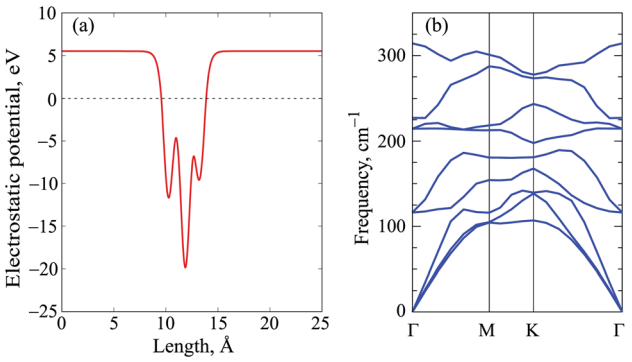

Fig. 2 Electrostatic potential along the c-axis (a) and phonon dispersion relations (b) of the Janus ZrSSe at equilibrium.

Table 1 Lattice constant a and bond lengths of the Zr–S d_{Zr-S} and Zr–Se d_{Zr-Se} (in Å of monolayers ZrS_2, $ZrSe_2$, and Janus ZrSSe). Calculated band gaps of the monolayers using PBE E_g^{PBE}, PBE + SOC $E_g^{PBE+SOC}$ and HSE E_g^{HSE} functionals are in eV

	a	d_{Zr-S}	d_{Zr-Se}	E_g^{PBE}	$E_g^{PBE+SOC}$	E_g^{HSE}
ZrS_2	3.699	2.584	—	1.104	—	1.871
$ZrSe_2$	3.790	—	2.697	0.479	—	1.079
ZrSSe	3.738	2.572	2.705	0.689	0.572	1.341

potential along the c-axis for the Janus ZrSSe. To examine the dynamic stability, the phonon spectrum of the Janus ZrSSe is calculated as shown in Fig. 2(b). From Fig. 2(b) we can see that there is no soft mode (negative frequency) in the phonon spectrum of the Janus ZrSSe. This indicates that, at equilibrium, the Janus ZrSSe is dynamically stable.

We first calculate the band structures and partial density of states (PDOS) of monolayers ZrS_2 and $ZrSe_2$ as shown in Fig. 3. We can see that both the ZrS_2 and $ZrSe_2$ are indirect semiconductors. The band gap of monolayer ZrS_2 is larger than that of monolayer $ZrSe_2$. At the PBE level, the band gaps of the monolayers ZrS_2 and $ZrSe_2$ are 1.104 eV and 0.479 eV, respectively. However, we know that, in the DFT calculations, the band gap problem of material depends greatly on the approach, *i.e.*, which functional is used in the calculations. The PBE functional underestimates the band gap of insulators and semiconductors.[34] The GW approximation[35] or Heyd–Scuseria–Ernzerhof (HSE06) hybrid functional[30] was expected to be a suitable method to solve the band gap problem of the materials. Therefore, to accurately calculate the energy gap of the ZrS_2, $ZrSe_2$ and Janus ZrSSe monolayers, in this study we use also the HSE06 hybrid functional to estimate their band structure. The band gap of the monolayers ZrS_2 and $ZrSe_2$ are, respectively, 1.871 eV and 1.079 eV at the HSE06 level, quite larger than that calculated by the PBE functional.

Band structure and PDOS of the Janus ZrSSe are shown in Fig. 4. We calculate the electronic structure of the Janus ZrSSe along the Γ–M–K–Γ high-symmetry direction in the energy region from −6 eV to 6 eV. As shown in Fig. 4, the Janus ZrSSe is an indirect semiconductor at equilibrium. The band gap of the Janus ZrSSe is $E_g^{PBE} = 0.689$ eV and $E_g^{HSE} = 1.341$ eV at the PBE and HSE06 levels, respectively. This result is in good agreement with previous calculations.[18] From Fig. 4, we can see that at the equilibrium state, the conduction band minimum (CBM) is located at the M-point, while the valence band maximum (VBM) is located at the Γ-point. Focusing on analyzing the formation of electronic bands of the Janus ZrSSe, we performed the calculations for its PDOS as depicted in the right panel of Fig. 4. The electronic bands of the Janus ZrSSe were formed mainly by the contribution of S-p, Se-p, and Zr-d orbitals. The contribution of Zr-d orbitals to the conduction band is quite large, particularly in the energy range from 2 eV to 4 eV. The contribution of S-p and Se-p orbitals to the valence band is quite balanced. While the contribution of the Se-p orbitals to the valence band is dominant in the energy region from 1 eV to 3 eV, the S-p orbitals have a significant contribution to the valence bands in the energy region from 3 eV to 4 eV. The contribution of the s-orbital of S, Se, and Zr atoms to the electronic bands is quite small compared to other orbitals. Overall, the conduction band is largely contributed to by the orbitals of Zr atoms while the orbitals of S and Se atoms provide the dominant contribution to the valence band.

The redox potential of water splitting is dependent on the pH value.[36] At pH = 00, the standard oxidation (O_2/H_2O) potential

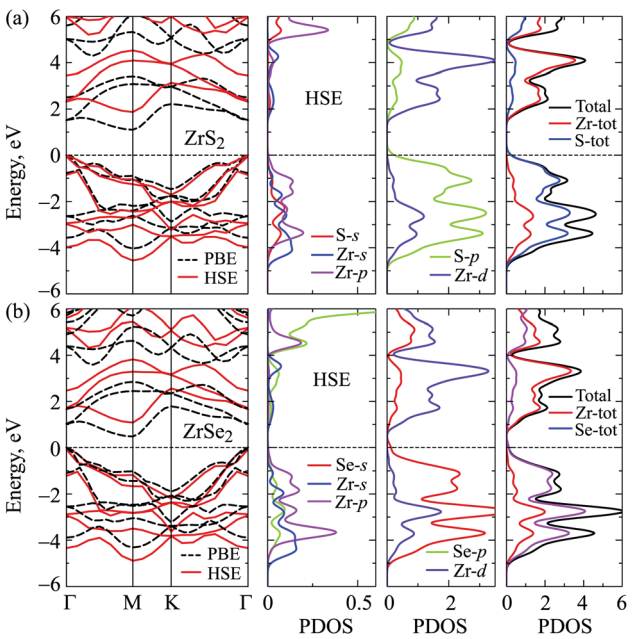

Fig. 3 Band structures and PDOS of the monolayers ZrS_2 (a), and $ZrSe_2$ (b). The Fermi level is set to be zero.

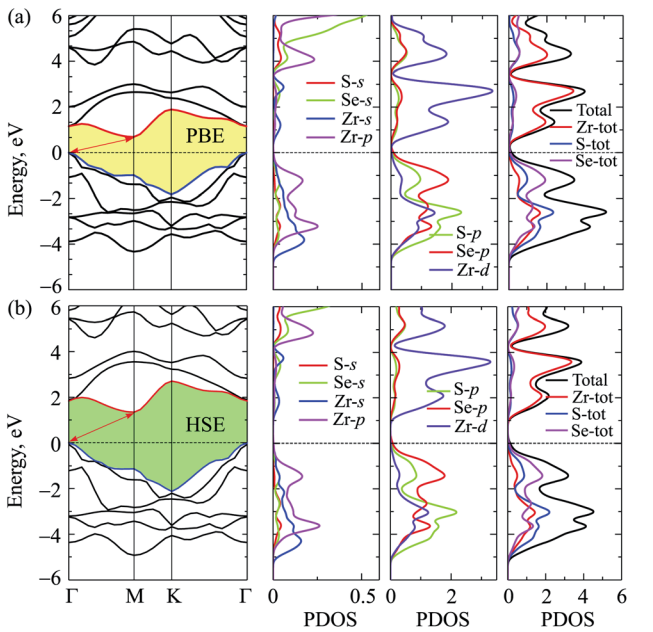

Fig. 4 Band structures and PDOS of the Janus ZrSSe at the PBE (a), and HSE (b) levels.

and reduction (H^+/H_2) potential for water splitting are $E_{oxi} = -5.67$ eV and $E_{red} = -4.44$ eV. In Fig. 5, we show the position of the CBM and VBM relative to the normal hydrogen electrode (NHE) of the ZrS_2, $ZrSe_2$ and Janus ZrSSe monolayers at pH = 0. The photocatalytic activity of the material depends greatly on the band gap. To possess the photocatalytic activity, the CBM must be higher than the standard hydrogen reduction potential of the H^+/H_2 and the VBM must be lower than the standard redox potential of the O_2/H_2O. At pH = 0, the standard oxidation potential of the O_2/H_2O is −5.67 eV *vs.* the vacuum level, or 1.23 eV *vs.* the NHE. This implies that to be able to possess photocatalytic activity, the minimum energy gap of the material must be at least 1.23 eV. As listed in Table 1, the band gaps of the ZrS_2 (1.871 eV) and Janus ZrSSe (1.341 eV) monolayers are larger than 1.23 eV at the HSE06 level. Then, we examined the possibility of photocatalytic activity of these monolayers for water splitting *via* calculations for band edge alignment. The VBM and CBM edge alignment of ZrS_2, $ZrSe_2$, and Janus ZrSSe monolayers are shown in Fig. 5. From Fig. 5, we see that the photocatalytic activity of the ZrS_2 monolayer is greatest. For the Janus ZrSSe, the VBM is right at the standard oxidation potential of the O_2/H_2O and the CBM is higher than the standard hydrogen reduction potential of the H^+/H_2. From this, we can conclude that, at the equilibrium state, the Janus ZrSSe monolayer possesses photocatalytic activity for water splitting applications.

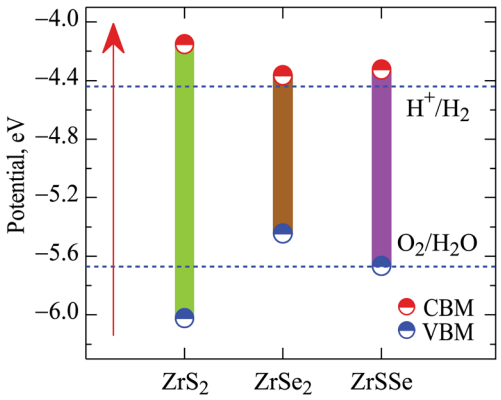

Fig. 5 The VBM and CBM edge alignment of ZrS_2, $ZrSe_2$, and Janus ZrSSe monolayers. The horizontal dashed lines refer to the standard potentials for water splitting at pH = 0.

Two-dimensional layered materials in general and monolayer transition metal dichalcogenides in particular, have electronic properties that are sensitive to external influences such as strain engineering or electric field. We next consider the effect of a biaxial strain, ε_b, on the electronic properties of the Janus ZrSSe. The calculations for the band structure of the strained Janus ZrSSe are performed at the PBE level. Band structures of the Janus ZrSSe under different levels of ε_b are shown in Fig. 6. Our DFT calculations demonstrate that in the presence of the tensile strain $\varepsilon_b > 0$ [see Fig. 6(a)], the Janus

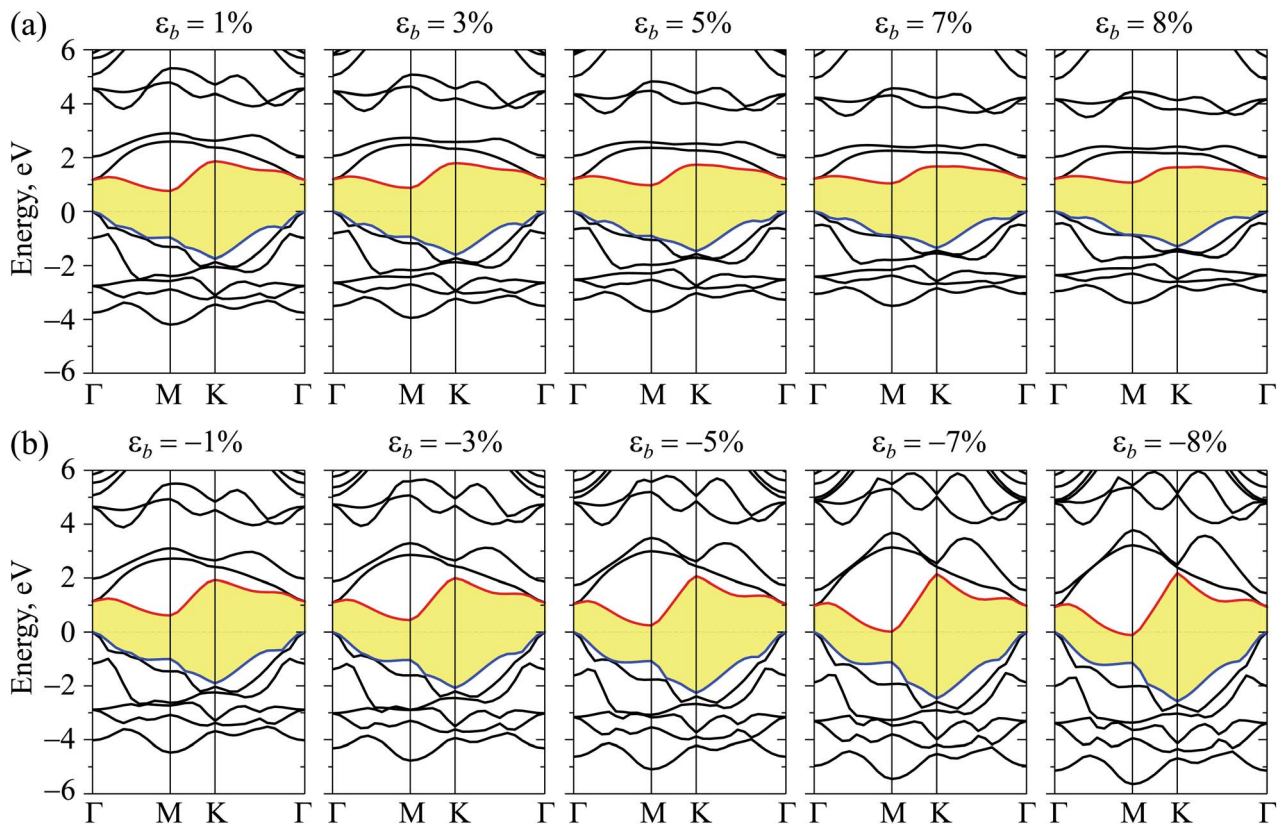

Fig. 6 Band structure of the Janus ZrSSe under different levels of (a) tensile, and (b) compressive biaxial strains.

ZrSSe is still a semiconductor with an indirect band gap. In this case, the CBM and VBM of the tensile strained Janus ZrSSe are always at the M- and Γ-points, respectively. The tensile strain leads to a slight increase in the energy gap of the Janus ZrSSe. Unlike the case of tensile strain, the effect of compression strain ($\varepsilon_b < 0$), as shown in Fig. 6(b), on the band structure of the Janus ZrSSe is significant. The energy gap of the Janus ZrSSe decreases quickly when the compression biaxial strain is introduced. More interestingly, semiconductor–metal transitions were observed in the Janus ZrSSe at large biaxial strain of $\varepsilon_b = -7\%$. The band gap of the Janus ZrSSe is equal to zero at the $\varepsilon_b = -7\%$ as depicted in Fig. 6(b).

To study the influence of an applied electric field E on the electronic properties of the Janus ZrSSe, the electric field is applied perpendicularly to the monolayer surface. The direction of $\vec{E}$ is along the c-axis. The negative field (minus sign) implies that the $\vec{E}$ is opposite to the c-axis. In contrast to the strain engineering, the influence of an external electric field on the band structure of the Janus ZrSSe is quite weak. As shown in Fig. 7, the band structure of the Janus ZrSSe is almost unchanged in the presence of the perpendicular electric field. Dependence of the band gap of the Janus ZrSSe on the strain engineering, ε_b, and external electric field E is depicted in Fig. 8. From Fig. 8, we can see that the electric field only slightly changes the band gap of the Janus ZrSSe. While a positive electric field increases its band gap slightly, a negative electric field reduces its energy. In the electric field from -5 V nm^{-1} to 5 V nm^{-1}, the energy gap depends linearly on the electric field. However, as mentioned above, this change is very small. The band gaps of the Janus ZrSSe at $E = -5$ V nm^{-1} and $E = +5$ V nm^{-1} are, respectively, 0.664 eV and 0.720 eV. Fig. 7 also shows that the tensile strain increases the band gap of the Janus ZrSSe. However, the gap tends to increase slowly at large ε_b. The band gap of the Janus ZrSSe reaches 1.074 eV at $\varepsilon_b = 8\%$. In the presence of biaxial strain, change tendency of the band gap of the Janus ZrSSe is similar to that of monolayer ZrS_2. A previous study indicates that while compressive biaxial strain reduces

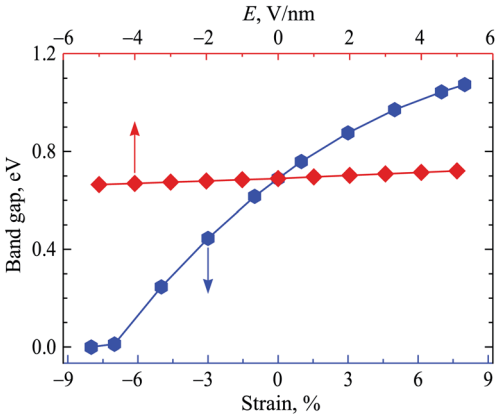

Fig. 8 Dependence of band gap of Janus ZrSSe on strain engineering and electric field E.

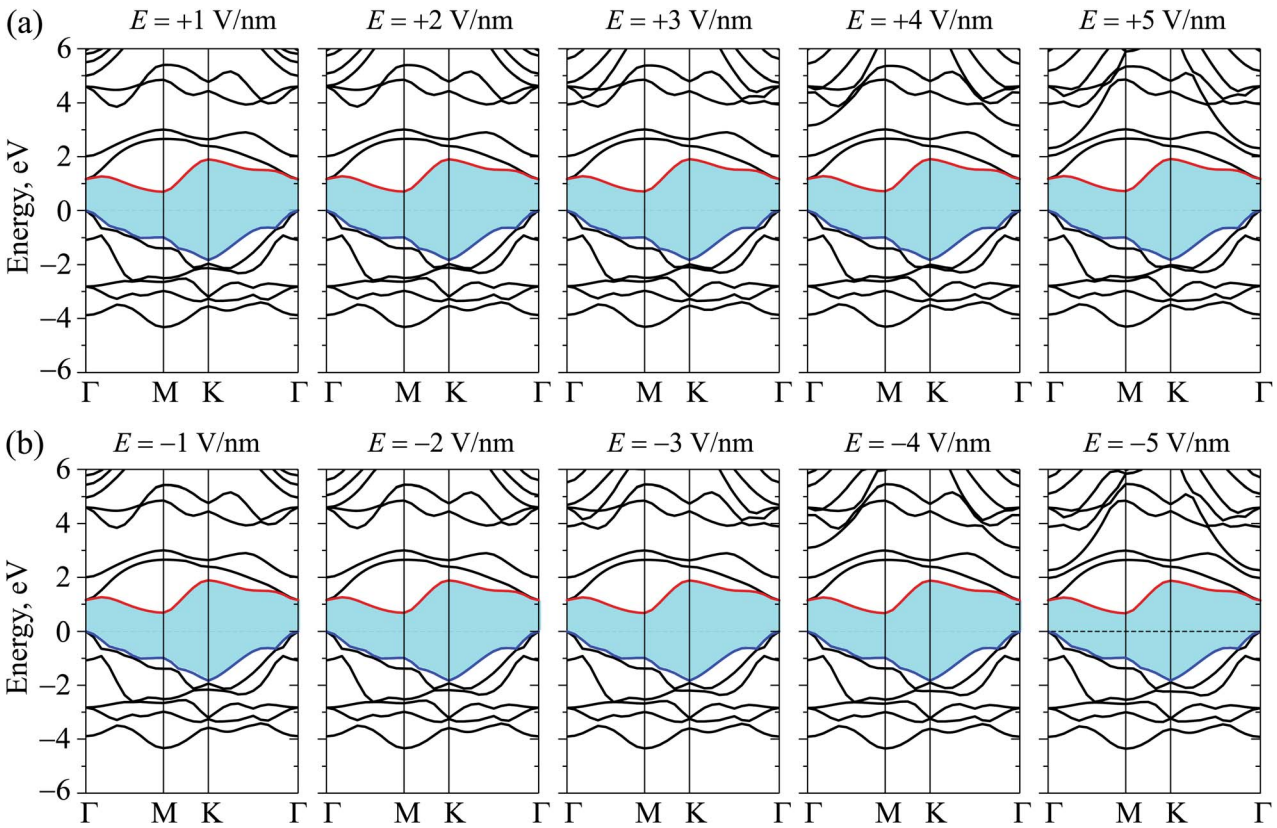

Fig. 7 Band structure of the Janus ZrSSe under (a) positive, and (b) negative, external electric fields.

the band gap of the monolayer ZrS_2, the band gap of the monolayer ZrS_2 is increased in the presence of tensile strain varying from 0 to 6%.[37] However, compared with other transition metal dichalcogenide monolayers, we found that in the presence of tensile strain, while the band gap of the Janus ZrSSe increased slightly, the band gap of the transition metal dichalcogenide monolayers, such as PdS_2, $PdSe_2$, and $PtSe_2$, was significantly reduced.[38,39] In both cases of strain engineering and external electric field, from Fig. 6 and 7, we see that the change of band gap is due to the change of the conduction band. Indeed, the highest energy value of the valence band is always at the Fermi level $E_F = 0$ and does not change in the presence of an electric field or biaxial strain. Controlling the band gap by strain, and particularly the occurrence of a semiconductor–metal transition due to strain engineering, can offer many opportunities for applications of the Janus ZrSSe in nanoelectronics technologies.

It is well-known that the effect of the SOC on electronic properties of 2D layered materials is very important. In this work, the band structure, including SOC effects, of the Janus ZrSSe has been calculated using the PBE + SOC. In Fig. 9(a) and (b), we plot the band structures of the Janus ZrSSe using the PBE and PBE + SOC along the K–Γ–M–K high-symmetry direction. Our calculations indicate that at the equilibrium state the band gap of the Janus ZrSSe is reduced from $E_g^{PBE} = 0.689$ eV to $E_g^{PBE+SOC} = 0.572$ eV when the SOC effect is included. Besides, a spin–orbit splitting energy $\Delta E = 0.212$ eV appeared at the high symmetry Γ-point in the valence band of the Janus ZrSSe monolayer. The effect of the biaxial strain and external electric field on the spin–orbit splitting value ΔE is also shown in Fig. 9(c). We can see that, similar to the band gap, the effect of the electric field on the spin–orbit splitting value ΔE is quite weak. Meanwhile, the influence of the SOC effect on band structure of the Janus ZrSSe is quite strong. The spin–orbit splitting values of the Janus ZrSSe at the $\varepsilon_b = 0$, $\varepsilon_b = -8\%$, and $\varepsilon_b = 8\%$ are 0.212 eV, 0.235 eV and 0.175 eV, respectively.

In this part, we consider the optical characteristics of the Janus ZrSSe under strain engineering, ε_b, and external electric field E. We focus only on the dielectric function $\varepsilon(\omega)$, and the absorption coefficient $\alpha(\omega)$ of the Janus ZrSSe. The dielectric function can be written as

$$\varepsilon(\omega) = \varepsilon_1(\omega) + i\varepsilon_2(\omega). \quad (1)$$

Usually, the imaginary part $\varepsilon_2(\omega)$ is estimated first by the sum of the occupied–unoccupied transitions. The real part $\varepsilon_1(\omega)$ can then be obtained *via* the Kramers–Kronig transformation. The imaginary part $\varepsilon_2(\omega)$ of the dielectric function can be written as follows[40,41]

$$\varepsilon_2^{ij}(\omega) = \frac{4\pi^2 e^2}{Vm^2\omega^2} \sum_{\vec{k}nn'\sigma} \left\langle \vec{k}n\sigma|p_i|\vec{k}n'\sigma \right\rangle \left\langle \vec{k}n'\sigma|p_j|\vec{k}n\sigma \right\rangle \times f_{\vec{k}n}\left(1 - f_{\vec{k}n'}\right)\delta\left(E_{\vec{k}n'} - E_{\vec{k}n} - \hbar\omega\right), \quad (2)$$

where ω is the angular frequency of the electromagnetic irradiation, m and e are, respectively, the mass and charge of the electron, $\vec{p}$ is the momentum operator, the $|\vec{k}n\sigma\rangle$ term refers to the wave-function of the crystal corresponding to energy, $E_{\vec{k}n}$. $\vec{k}$ is the wave-vector and $f_{\vec{k}n}$ is the function of the Fermi distribution.

The absorption coefficient $\alpha(\omega)$ can be calculated using the dielectric function which can be expressed as[41,42]

$$\alpha(\omega) = \frac{\sqrt{2}\omega}{c}\left[\sqrt{\varepsilon_1^2(\omega) + \varepsilon_2^2(\omega)} - \varepsilon_1(\omega)\right]^{1/2}. \quad (3)$$

In our calculations, the incident light is polarized along the a-axis (parallel polarization) and is in the energy range from 0 to 10 eV. The calculated dielectric function of the Janus ZrSSe under biaxial strain, ε_b, and external electric field, E, is depicted in Fig. 9. We first focus on the effect of the ε_b on the dielectric function of the Janus ZrSSe as shown in Fig. 10(a). As shown in the imaginary part $\varepsilon_2(\omega)$ [bottom panel of Fig. 10(a)], the first optical gap of the Janus ZrSSe is at 1.892 eV. It is in the visible light region. Our calculations demonstrate that the first optical gap of the Janus ZrSSe is significantly shifted under the effects of strain engineering, ε_b. While the compressive strain causes

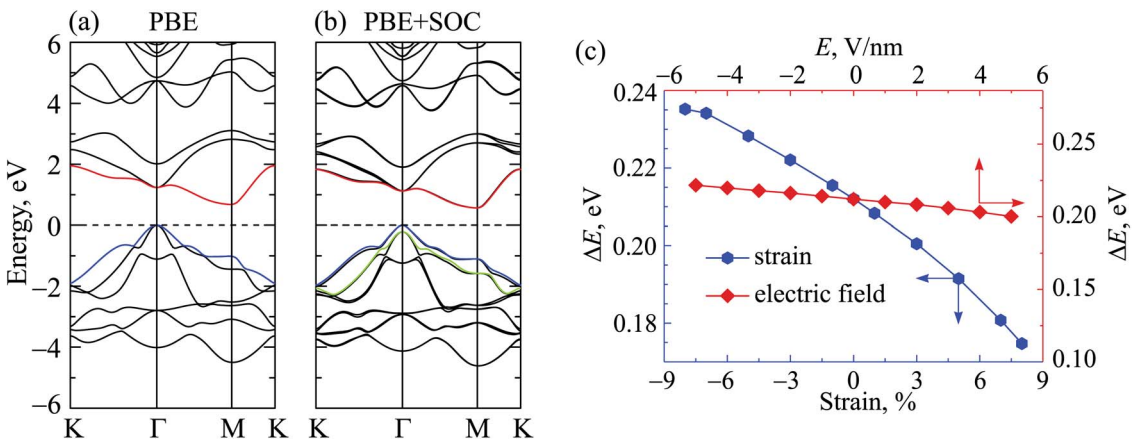

Fig. 9 Calculated band structures of the Janus ZrSSe using (a) PBE, and (b) PBE + SOC methods. Effect of biaxial strain and electric field on the spin–orbit splitting value ΔE at the Γ-point using PBE + SOC of the Janus ZrSSe (c).

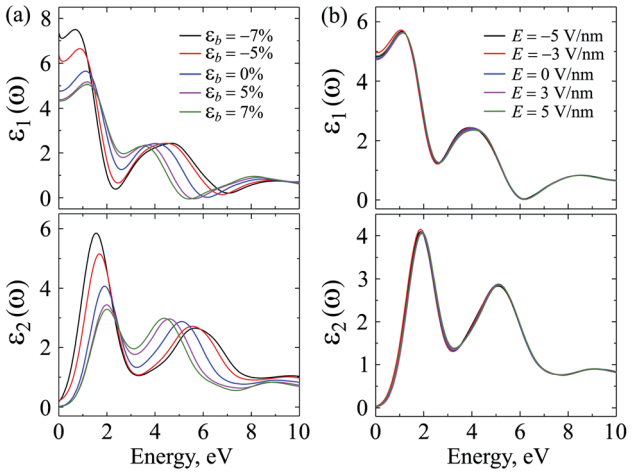

Fig. 10 Dielectric function parts of Janus ZrSSe under (a) biaxial strain, and (b) electric field.

the first optical gap of the Janus ZrSSe to move towards the lower energy region, the tensile strain causes it to move towards the higher energy region. The tendency of the first optical gap of the Janus ZrSSe in the case of tensile strain is the opposite of that of the transition-metal dichalcogenide monolayers such as PdS_2, $PdSe_2$, and $PtSe_2$, where both compressive and tensile strain cause the first optical peak to move towards the lower energy region.[38] It is well-known that the $\varepsilon_2(\omega)$ part of the $\varepsilon(\omega)$ is directly related to the absorption coefficient. Therefore, the optical gaps in the absorption spectrum of the Janus ZrSSe that we will discuss below will be closely related to this shifting. Similar to the electronic properties, the optical characteristics of the Janus ZrSSe are almost unaffected by the external electric field. Fig. 10(b) shows that parts of the dielectric constant are almost independent of the electric field, especially in the high energy region.

In Fig. 11, we show the calculated absorption coefficient $\alpha(\omega)$ in the presence of the biaxial strain, ε_b, and external electric field, E. From Fig. 11, we can see that the Janus ZrSSe can sustainably absorb both visible and ultraviolet light. In the case of without strain or electric field, the maximum absorption coefficient is 9.483×10^4 cm^{-1} at the incident light energy of 5.795 eV. As mentioned-above, the optical gaps of the Janus ZrSSe shift with strain energy, ε_b, and the absorption coefficient also greatly depends on strain energy. Fig. 11 demonstrates

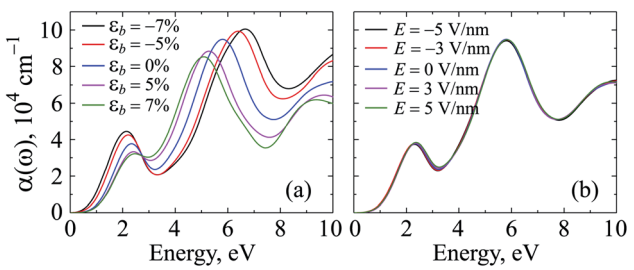

Fig. 11 Absorption coefficient $\alpha(\omega)$ of Janus ZrSSe under (a) biaxial stain, and (b) electric field.

that, while the tensile strain reduces maximum absorption coefficient, $\alpha(\omega)_{max}$, the compressive strain increases the $\alpha(\omega)_{max}$ significantly. The maximum coefficient at $\varepsilon_b = -7\%$ is up to 1.005×10^5 cm^{-1} at the incident light energy of 6.672 eV. From Fig. 10(b) and 11(b), we can conclude that the effect of the external electric field on the optical characteristics of the Janus ZrSSe is negligible. With the ability to absorb light in both the visible and ultraviolet range, especially with high absorption coefficient, we believe that Janus ZrSSe has a lot of potential for applications in optoelectronic devices.

4 Conclusion

In summary, we systematically investigated the electronic and optical properties of the Janus ZrSSe monolayer under strain engineering and an external electric field using DFT calculations. Our calculated results demonstrate that the Janus ZrSSe is an indirect semiconductor and it can absorb both visible light and ultraviolet light. Interestingly, at the equilibrium state, the Janus ZrSSe possesses photocatalytic activity for water splitting. The effect of strain engineering on the electronic and optical properties of the Janus ZrSSe monolayer is significant, especially the semiconductor–metal transition which can be observed at certain ε_b. Besides, the biaxial strain is the cause of shifting optical gaps and the significantly changing absorption coefficient of the Janus ZrSSe monolayer. Possessing photocatalytic activities and being able to control electronic properties by strain engineering, the Janus ZrSSe monolayer has many advantages in its application prospects in nanoelectronic devices and water splitting technologies.

Conflicts of interest

There are no conflicts to declare.

Acknowledgements

This research is funded by the Viet Nam National Foundation for Science and Technology Development (NAFOSTED) under Grant No. 103.01-2017.309.

References

1 K. S. Novoselov, A. K. Geim, S. V. Morozov, D. Jiang, Y. Zhang, S. V. Dubonos, I. V. Grigorieva and A. A. Firsov, *Science*, 2004, **306**, 666.
2 C. V. Nguyen, N. N. Hieu, N. A. Poklonski, V. V. Ilyasov, L. Dinh, T. C. Phong, L. V. Tung and H. V. Phuc, *Phys. Rev. B*, 2017, **96**, 125411.
3 C. V. Nguyen, N. N. Hieu, C. A. Duque, D. Q. Khoa, N. V. Hieu, L. V. Tung and H. V. Phuc, *J. Appl. Phys.*, 2017, **121**, 045107.
4 P. T. T. Le, K. Mirabbaszadeh, M. Davoudiniya and M. Yarmohammadi, *Phys. Chem. Chem. Phys.*, 2018, **20**, 25044.
5 C. V. Nguyen, N. N. Hieu, D. Muoi, C. A. Duque, E. Feddi, H. V. Nguyen, L. T. T. Phuong, B. D. Hoi and H. V. Phuc, *J. Appl. Phys.*, 2018, **123**, 034301.

6 T. V. Vu, A. A. Lavrentyev, D. V. Thuan, C. V. Nguyen, O. Y. Khyzhun, B. V. Gabrelian, K. C. Tran, H. L. Luong, P. D. Tung, K. D. Pham, P. T. Dang and D. D. Vo, *Superlattices Microstruct.*, 2019, **125**, 205–213.
7 K. D. Pham, N. N. Hieu, H. V. Phuc, I. A. Fedorov, C. A. Duque, B. Amin and C. V. Nguyen, *Appl. Phys. Lett.*, 2018, **113**, 171605.
8 K. D. Pham, L. G. Bach, B. Amin, M. Idrees, N. N. Hieu, H. V. Phuc, H. D. Bui and C. V. Nguyen, *J. Appl. Phys.*, 2019, **125**, 225304.
9 P. T. T. Le, N. N. Hieu, L. M. Bui, H. V. Phuc, B. D. Hoi, B. Amin and C. V. Nguyen, *Phys. Chem. Chem. Phys.*, 2018, **20**, 27856.
10 H. V. Phuc, V. V. Ilyasov, N. N. Hieu, B. Amin and C. V. Nguyen, *J. Alloys Compd.*, 2018, **750**, 765.
11 J. Zhang, S. Jia, I. Kholmanov, L. Dong, D. Er, W. Chen, H. Guo, Z. Jin, V. B. Shenoy, L. Shi and J. Lou, *ACS Nano*, 2017, **11**, 8192.
12 A.-Y. Lu, H. Zhu, J. Xiao, C.-P. Chuu, Y. Han, M.-H. Chiu, C.-C. Cheng, C.-W. Yang, K.-H. Wei, Y. Yang, Y. Wang, D. Sokaras, D. Nordlund, P. Yang, D. A. Muller, M.-Y. Chou, X. Zhang and L.-J. Li, *Nat. Nanotechnol.*, 2017, **12**, 744.
13 L. Dong, J. Lou and V. B. Shenoy, *ACS Nano*, 2017, **11**, 8242.
14 A. Huang, W. Shi and Z. Wang, *J. Phys. Chem. C*, 2019, **123**, 11388.
15 N. N. Som and P. K. Jha, *Int. J. Hydrogen Energy*, 2019, DOI: 10.1016/j.ijhydene.2019.09.033.
16 W.-L. Tao, Y. Mu, C.-E. Hu, Y. Cheng and G.-F. Ji, *Philos. Mag.*, 2019, **99**, 1025.
17 Z. Zeng, Z. Yin, X. Huang, H. Li, Q. He, G. Lu, F. Boey and H. Zhang, *Angew. Chem., Int. Ed.*, 2011, **50**, 11093.
18 S.-D. Guo, Y.-F. Li and X.-S. Guo, *Comput. Mater. Sci.*, 2019, **161**, 16.
19 Q. Zhao, Y. Guo, K. Si, Z. Ren, J. Bai and X. Xu, *Phys. Status Solidi B*, 2017, **254**, 1700033.
20 Q. Xin, X. Zhao, X. Ma, N. Wu, X. Liu and S. Wei, *Phys. E*, 2017, **93**, 87.
21 Y. Li, J. Kang and J. Li, *RSC Adv.*, 2014, **4**, 7396.
22 Dimple, N. Jena, A. Rawat, R. Ahammed, M. K. Mohanta and A. De Sarkar, *J. Mater. Chem. A*, 2018, **6**, 24885.
23 S.-D. Guo and J. Dong, *Semicond. Sci. Technol.*, 2018, **33**, 085003.
24 S.-D. Guo, X.-S. Guo, R.-Y. Han and Y. Deng, *Phys. Chem. Chem. Phys.*, 2019, **21**, 24620.
25 P. Giannozzi, S. Baroni, N. Bonini, M. Calandra, R. Car, C. Cavazzoni, D. Ceresoli, G. L. Chiarotti, M. Cococcioni, I. Dabo, A. D. Corso, S. de Gironcoli, S. Fabris, G. Fratesi, R. Gebauer, U. Gerstmann, C. Gougoussis, A. Kokalj, M. Lazzeri, L. Martin-Samos, N. Marzari, F. Mauri, R. Mazzarello, S. Paolini, A. Pasquarello, L. Paulatto, C. Sbraccia, S. Scandolo, G. Sclauzero, A. P. Seitsonen, A. Smogunov, P. Umari and R. M. Wentzcovitch, *J. Phys.: Condens. Matter*, 2009, **21**, 395502.
26 P. E. Blöchl, *Phys. Rev. B: Condens. Matter Mater. Phys.*, 1994, **50**, 17953.
27 J. P. Perdew, K. Burke and M. Ernzerhof, *Phys. Rev. Lett.*, 1996, **77**, 3865.
28 J. P. Perdew, K. Burke and M. Ernzerhof, *Phys. Rev. Lett.*, 1997, **78**, 1396.
29 A. H. MacDonald, W. E. Picket and D. D. Koelling, *J. Phys. C: Solid State Phys.*, 1980, **13**, 2675.
30 J. Heyd, G. E. Scuseria and M. Ernzerhof, *J. Chem. Phys.*, 2003, **118**, 8207.
31 S. Grimme, *J. Comput. Chem.*, 2006, **27**, 1787.
32 M. J. Mleczko, C. Zhang, H. R. Lee, H.-H. Kuo, B. Magyari-Köpe, R. G. Moore, Z.-X. Shen, I. R. Fisher, Y. Nishi and E. Pop, *Sci. Adv.*, 2017, **3**, e1700481.
33 C.-F. Fu, J. Sun, Q. Luo, X. Li, W. Hu and J. Yang, *Nano Lett.*, 2018, **18**, 6312.
34 J. P. Perdew and M. Levy, *Phys. Rev. Lett.*, 1983, **51**, 1884.
35 L. Hedin, *Phys. Rev.*, 1965, **139**, A796.
36 K. Ren, C. Ren, Y. Luo, Y. Xu, J. Yu, W. Tang and M. Sun, *Phys. Chem. Chem. Phys.*, 2019, **21**, 9949.
37 H. Y. Lv, W. J. Lu, D. F. Shao, H. Y. Lu and Y. P. Sun, *J. Mater. Chem. C*, 2016, **4**, 4538.
38 S. Deng, L. Li and Y. Zhang, *ACS Appl. Nano Mater.*, 2018, **1**, 1932.
39 Y.-S. Lan, Q. Lu, C.-E. Hu, X.-R. Chen and Q.-F. Chen, *Appl. Phys. A*, 2019, **125**, 33.
40 A. Delin, P. Ravindran, O. Eriksson and J. Wills, *Int. J. Quantum Chem.*, 1998, **69**, 349.
41 S. Z. Karazhanov, P. Ravindran, A. Kjekshus, H. Fjellvag and B. G. Svensson, *Phys. Rev. B: Condens. Matter Mater. Phys.*, 2007, **75**, 155104.
42 P. Ravindran, A. Delin, B. Johansson, O. Eriksson and J. M. Wills, *Phys. Rev. B: Condens. Matter Mater. Phys.*, 1999, **59**, 1776.